Solar Large-Scale Channeled Dimmings Produced by Coronal Mass Ejections

I. M. Chertok and V. V. Grechnev

Institute of Terrestrial Magnetism, Ionosphere, and Radiowave Propagation, Russian Academy of Sciences,
Troitsk, Moscow oblast, 142190 Russia
Institute for Solar–Terrestrial Physics, P.O. Box 4026, Irkutsk, 664033 Russia
Received June 13, 2002; in final form, August 21, 2002

Abstract—A new type of dimmings, or transient coronal holes (i.e., regions of reduced soft-X-ray and EUV emission), is revealed in analyses of difference solar images obtained with the SOHO EIT ultraviolet telescope at 195 Å. Such features can be observed on the solar disk after halo-type coronal mass ejections (CMEs). If several active regions, filaments, and other structures are present on the disk during a major eruptive event, then strongly anisotropic, channel-shaped ("channeled") dimmings coexist with relatively compact dimmings adjacent to the eruption center. The channeled dimmings are comparable to the compact dimmings in terms of their contrast; stretch along several narrow, extended features (channels); and can span nearly the entire visible disk. Coronal waves, which appear as fronts of enhanced brightness traveling ahead of the dimmings in some halo CME events, are also anisotropic. We argue that such transient phenomena are closely related to the strong disturbance and restructuring of large-scale magnetic fields involved in CMEs, and the channeled character of the dimmings reflects the complexity of the global solar magnetosphere, in particular, near the solar-activity maximum. © *2003 MAIK "Nauka/Interperiodica".*

1. INTRODUCTION

Coronal mass ejections (CMEs) are the largest-scale phenomena of sporadic solar activity, which play an important, and frequently determining, role in various solar, interplanetary, and geophysical events (see, e.g., reviews [1−6] and references therein). While flares release energy stored in the local magnetic fields of active regions, the origin of CMEs is most likely rooted in the dynamics of large-scale magnetic fields, the global evolution of the solar magnetosphere, and the instabilities of individual magnetospheric structures, such as coronal streamers, prominences (filaments), large arcades, etc. Considerable progress in studying CMEs has been achieved in recent years, primarily due to Yohkoh [7] and SOHO [8] observations.

CMEs rising in the corona at velocities of up to 2000 km/s are observed in white light with the SOHO LASCO coronagraph [9] over the limb, at heliocentric distances of up to $30R_S$ (where R_S is the solar radius), due to the scattering of photospheric radiation by free electrons, whose density is substantially increased in the ejected material. In many cases, the CMEs far exceed the optical solar disk in size, even at small heliocentric distances. The transequatorial character and global scale of CMEs are visible, for example, in the association of the footpoints of loop transients observed in many big events with structures located in opposite (northern and southern) hemispheres of the Sun.

Observations of disk processes before, during, and after the eruption are very informative for studies of CMEs. High-quality images obtained with the Yohkoh SXT [10] and SOHO EIT [11] telescopes indicate that CME-related substantial restructurings and large-scale magnetic-field disturbances are most clearly manifest in so-called dimmings and coronal waves. Dimmings, or transient coronal holes [12−17], are regions of reduced soft X-ray and EUV intensity with lifetimes of several to several tens of hours that are formed after the CMEs near the eruption center—e.g, at the periphery of the sigmoid structure—and can cover a large portion of the solar disk. Analyses show [15, 16] that the most intense dimmings are observed simultaneously in several UV lines (FeIX/X 171 Å, FeXII 195 Å, FeXV 284 Å) that are sensitive to coronal plasma at temperatures of $(1.2−2.0) \times 10^6$ K, as well as in soft X-rays, corresponding to temperatures $> 2.5 \times 10^6$ K. Therefore, dimmings can be interpreted as a result of the complete or partial opening of the magnetic fields in these structures, with the evacuation of material and a corresponding reduction in their intensity. Fairly frequently, a bright front can be observed ahead of the developing dimmings, indicative of a coronal or EIT wave traveling from the eruption center at a speed

of several hundred km/s [15,18–20]. According to one point of view [19, 21, 22], the EIT wave is a CME-initiated MHD disturbance—a coronal analog of the chromospheric Moreton wave observable in the H_α line [23]. Another interpretation [24, 25] is that the coronal wave is associated with the evolution of magnetic structures involved in the CME, in particular, with the compression of plasma at the advancing boundary of the dimming—a region of opening magnetic field lines.

It is currently believed that dimmings and coronal waves are mainly quasi-isotropic and propagate in a wide-angle sector more or less symmetrically with respect to the eruption center [15, 19, 21, 22]. At the same time, coronal waves are known to be reflected and refracted as they interact with the strong magnetic fields of active regions [26]; a dimming may encompass separate large-scale (including transequatorial) loops anchored in the eruption region [17–29]. In some cases, so-called twin dimmings are observed, with the strongest intensity decreases occurring in two regions adjacent to the eruption center and located symmetrically with respect to the polarity-reversal line and the posteruptive arcade [15, 16]. Such twin dimmings appear to be the footpoints of large-scale flux lope structures erupting during the CME. The eruptive events accompanied by coronal waves and dimmings currently described in the literature occurred primarily in 1997 and 1998, during the growth phase of the current activity cycle—a period when the global solar magnetosphere had a relatively simple structure.

We present here our analyses of the spatial structure of UV dimmings observed near the activity-cycle maximum, when the solar magnetosphere was fairly complex. Difference SOHO EIT heliograms obtained at 195 Å indicate that the eruption of a large CME against the background of several active regions and other features on the disk is accompanied by clearly defined, anisotropic, channel-shaped ("channeled") dimmings that develop along narrow, extended features (channels) and stretch between widely spaced activity centers that can cross the heliographic equator. Methodological questions connected with identifying dimmings are discussed in Section 2. Section 3 begins with a consideration of a quasi-isotropic coronal wave and dimming that are typical for a relatively simple large-scale magnetic-field structure. Further, we consider in detail the development and structure of dimmings observed during two halo CME events in January and February 2000 when the global solar magnetosphere had a complex structure. A discussion and concluding remarks are presented in Section 4.

2. METHODOLOGICAL NOTES

In analysis of the large-scale structure of dimmings, it is reasonable to consider halo CME events in which the eruption source is located in the central zone of the visible disk, and the earthward traveling CME is observed as a bright and expanding emitting region surrounding the entire occulting disk of the coronagraph [30]. It is reasonable to use SOHO EIT 195 Å data, because heliograms are taken with the highest cadence (normally, 12–20 min) just in this line [11]. Corresponding FITS files are available in the EIT catalogue at http://umbra.nascom.nasa.gov/eit/eit-catalog.html.

Studies of dynamic events on the solar disk, particularly events such as coronal waves and dimmings, are based on two types of difference images [15–18]. Running difference (RD) images are obtained by subtracting the preceding heliogram from the current heliogram. Fixed difference (FD) images are computed by subtracting a single pre-event image of the sun from all subsequent heliograms. In such difference images (Fig. 1), dimmings are manifest as dark features with reduced intensity, while coronal waves appear as bright advancing fronts.

There are substantial differences between the RD and FD images [in Fig. 1, panels (a) and (c) should be compared to (b) and (d)]. The RD images emphasize changes (in the brightness, localization, and structure of sources) that have occurred during the interval between contiguous frames. In particular, the front of the traveling coronal wave can be most clearly seen in the RD images. However, many artifacts unavoidably appear in the RD images. For example, dark features—spurious dimmings of a methodological origin—will be seen where there was a bright, advancing coronal-wave front and its fragments in the previous RD frame. A similar spurious dimming will appear in an RD image when the intensity of a bright feature decreases, in particular, if such a feature appears during a flare or posteruptive phase. Likewise, if the depth of a true dimming decreases with time, a spurious brightening will be seen in the next RD frame at the same place. If, however, the intensity of a true brightening or dimming remains nearly unchanged between contiguous frames, the corresponding feature will be completely missing from the RD image (the region will have the background intensity). The artifacts described above can be identified by scrutinizing the RD images in Figs 1a and 1c. In particular, many of the brightenings and dimmings visible behind the coronal-wave front in Figs 1a and 1c have a methodological origin and are due to the procedure used to obtain the RD images.

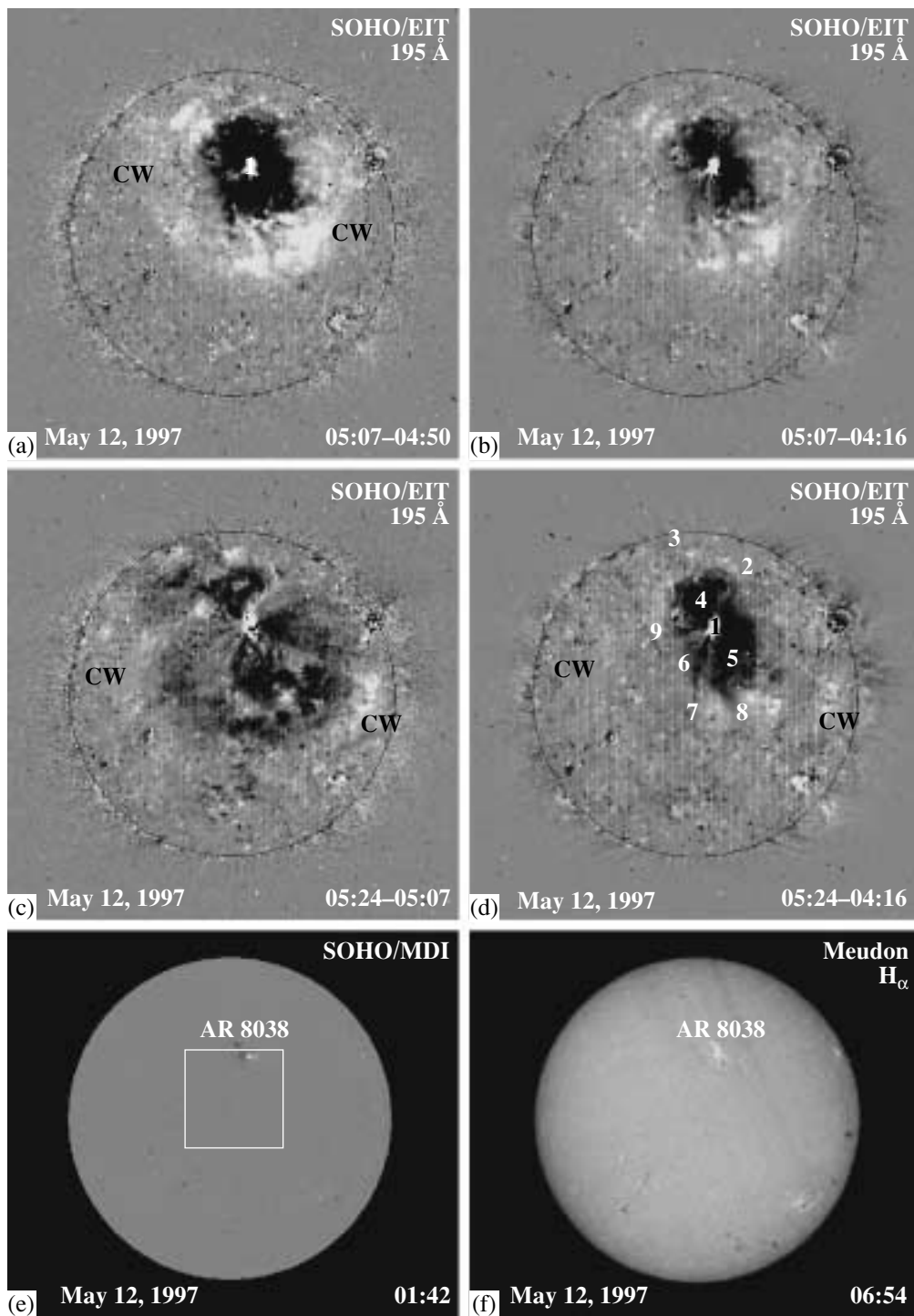In FD images (Figs 1b, 1d), changes that occur during the event are clearly visible, in particular, those

Fig. 1. (a, c) Running and (b, d) fixed difference images of the Sun in the 195 Å line (SOHO EIT). These illustrate the differences between the two image types and the quasi-isotropic character of the dimming and coronal wave (CW) after the halo CME of May 12, 1997. The (e) SOHO MDI magnetogram and (f) H$_\alpha$ heliogram demonstrate the presence of only one large active region on the disk.

related to coronal waves and dimmings (naturally, we mean here changes relative to the selected reference frame chosen before the event). However, the construction of FD images raises another problem,

since solar rotation can also produce spurious features. In 512×512 SOHO EIT frames [11] with a pixel size of 5.24″, the effect of rotation is virtually indistinguishable if the RD images are obtained by

subtracting images taken 12–20 min apart. However, the rotation of the solar surface becomes important if the interval between frames is several tens of minutes or several hours, as in the case of constructing FD images. In particular, it is clear that the angular displacement of a dark feature observed in absorption will give rise to a spurious bright edge in the difference image to the east of this feature. In contrast, a bright feature observed in emission will produce a dark eastern edge resembling a dimming. This effect is especially pronounced for narrow, meridionally stretched features, e.g., vertical filaments and transequatorial loops, when the longitudinal extent of the spurious edge is comparable to the size of the feature itself. To suppress the formation of spurious features, we introduced corrections to compensate for the solar rotation before constructing the difference images, aligned the heliograms, and reduced them to a unified calibration. As a rule, all the frames considered were rerotated to the time of the same reference (pre-event) heliogram, which was subtracted from the subsequent frames to obtain the FD images. For example, this time is 04:16 UT for Figs. 1b and 1d.

In this study, we will analyze dimmings using FD images with a preliminary compensation for solar rotation. We will use RD images as an additional source of information to examine some changes detected in the FD heliograms in more detail. In this context, the most effective tool for the analysis and representation of data is computer movies composed of difference images and viewed in JAVA format with adjustable frame rate and playing direction. Some examples of such movies, as well as other illustrations of CMEs related to the events considered, can be found at http://helios.izmiran.troitsk.ru/lars/Chertok/dimming/index.html.

The following important point deserves particular attention. The dimmings analyzed here and, especially, individual fragments of their large-scale structure, as well as many coronal waves, are relatively faint phenomena (see below). For this reason, we have limited the intensity range in the difference images in order to make these features sufficiently pronounced. As a result, the brightest sources (particularly those emerging during flares), which are not the subject of our analysis, are saturated. A similar approach has been used to identify large-scale emitting chains in microwave, UV, and X-ray heliograms [31]. For example, the brightness cutoffs for the RD and FD images shown in Fig. 1 are ±75 and ±150 count/pixel, respectively. Similar intensity ranges were used for the other events under study. Naturally, the outlines and some structural details of dimmings and coronal waves vary to some extent depending on the chosen intensity range. Finally, we note that, if the time interval between the current and reference heliograms

is long, regular vertical strips of an instrumental origin can be detected in high-sensitivity FD images (Fig. 1d).

In the SOHO EIT images, periodic vertical and horizontal light strips due to the properties of the CCD matrix used are not uncommon [11]. Rotation of the solar image does not affect the positions of the horizontal strips but displaces the vertical strips. For this reason, the subtraction of images suppresses the horizontal strips and enhances the vertical ones. Since the rotation is performed only for a spherical surface, this instrumental and methodological effect, which is exaggerated by the intensity cutoff, is present only on the solar disk.

3. ANALYSES OF PARTICULAR EVENTS

3.1. Event of May 12, 1997

We restrict ourselves to brief remarks about this event, since it is well known and is described in detail in the literature [15, 17, 32, 33]. We present it here as an illustration of CME-related disturbances that occur under relatively simple conditions in the global solar magnetosphere; Fig. 1, which refers to this event, was already used in the discussion of the analysis techniques (Section 2).

The eruption source was located in AR 8038 (N21 W09), which was essentially the only active region on the solar disk at that time. This can be seen from the SOHO MDI magnetogram and H_α heliogram of the Observatoire de Paris shown in Figs 1e and 1f. As far as other significant features are concerned, only the northern and southern coronal holes (CHs) could be observed on the disk in soft X rays with the Yohkoh SXT telescope and were present in the original UV heliograms taken in the 195 and 284 Å lines [15]. This event was associated with a long-duration flare of class 1F/C1.3 with its maximum near 04:50 UT. The CME recorded by the SOHO LASCO coronagraph was classified as a full halo emitting everywhere around the occulting disk, but its brightness was maximum over the eastern, western, and northern limb sectors [32].

The eruption of the CME was accompanied by pronounced, large-scale transient disturbances on the disk, in particular, a coronal wave and dimmings [13]. The difference heliograms obtained at 195 Å (Fig. 1) show that the coronal-wave front had a fragmentary structure but traveled more or less isotropically with respect to the eruption center 1. The front's propagation decelerated only as the northern polar CH was approached, and the interaction of the front with the CH gave rise to the long emitting chain 2–3 (Fig. 1d), which gradually encompassed the entire CH boundary and was observed over several

hours. Before its interaction with the CH, the coronal wave propagated over the solar surface at nearly the same velocity, 240 km/s, in all directions [15]. The halo CME had a similar velocity in the plane of the image [32].

The two deepest, symmetric twin dimmings with similar sizes and shapes (4, 5) formed northeast and southwest of the eruption center and were clearly visible in at least three UV lines—171, 195, and 284 Å—as well as in soft X rays [15]. It is important that, during the entire event, these intense dimmings were surrounded by a much weaker dimming region, which completely filled the space between the dimmings (4, 5) and the traveling quasi-isotropic coronal wave. Therefore, the weak dimming was also quasi-isotropic. It can be distinguished in two UV images (Figs. 1b, 1d), but is most pronounced in Fig. 5c in [17].

Thus, in this case, both the coronal wave and the dimmings were quasi-isotropic and covered the visible hemisphere almost entirely. It is likely that this character for the transient disturbances was due to the fact that only one active region was present on the disk at that time, so that the structure of the solar magnetosphere was fairly simple. In any case, as will be shown below, dimmings observed under more complex conditions are appreciably anisotropic and take the form of long, narrow features (channels). In fact, some signatures of such channels can be detected in the May 12, 1997 event; in particular, short dimming branches (1−6−7, 6−8, 1−9) can be distinguished in Fig. 1d.

3.2. Event of January 18, 2000

This event occurred when several active centers, filaments, and CHs were observed on the disk (Figs. 2e, 2f), so that the structure of the global solar magnetosphere was fairly complex. The event included a long-duration class 1N/M3.9 flare in region AR 8831 (S19 E11), with a maximum at 17:27 UT and a structured halo CME, which initially developed over the eastern limb and subsequently extended to all position angles.

The FD images at 195 Å obtained using a reference heliogram of 16:48 UT and shown in Figs 2a−2d demonstrate that, by 17:24 UT (Fig. 2a), a narrow transequatorial strip dimming formed along with an annular dimming surrounding the eruption center 1; the strip extended to region 2 in the southern half of the disk near the central meridian. In the next frame at 17:36 UT (Fig. 2b), this strip extends further westward to point 3. The dimming channel 1−4 going from the eruption center to the southeastern limb also becomes visible. A relatively faint branch of the

dimming 5−6−7 forms to the west of AR 8831 and is linked by the brightened loop 6−8 to the southwestern region, where another remote dimming center can be distinguished. The faint dimming 6−9 stretches to the southern limb region.

Subsequent frames, including the frame of 18:12 UT (Fig. 2c), clearly demonstrate the southeastern dimming loop 1−10, which may extend to limb 11. Furthermore, another, eastern, transequatorial dimming feature 12−13−14 can be distinguished, extending toward the active region located in the northeastern quadrant. The main eastern and western transequatorial dimming branches are linked by additional dimming features: one or two narrow strips of the dimming 2−14 pass near the central and northeastern activity complexes of the northern hemisphere (having extensions from region 14 in the form of narrow eastward and southeastward offshoots); another, more diffuse and possibly looplike dimming system 13−15 is located near the central meridian and joins the bright dimming 15−6, which fringes the eruption center from the north and northwest.

Virtually all these elements of channeled dimmings are also present in the last frame presented, of 18:36 UT (Fig. 2d). Note also the emergence of the relatively faint dimmings 14−16 and 17−18 stretching to the northeastern limb. The narrow dimming 10−11 going southward from the southeastern dimming loop can also be seen.

The relative depths and temporal changes in different portions of the channeled dimmings can be seen in Fig. 3. Selected $53'' \times 53''$ areas of various structures of dimming features (1−5) are marked in the heliogram (Fig. 3a), together with the region of the southern CH (6) for comparison. The corresponding time-variation profiles shown in Fig. 3b indicate that the intensity reduction in main dimmings that are both adjacent to the eruption center and channel-shaped is 25−80%. In area 4, some increase in intensity can be noted after a relatively brief, deep dimming. Curve 6 confirms that the dimming does not involve the southern polar CH. As can be seen from Fig. 3b, the development time for dimmings, including channeled dimmings, is several tens of minutes. The total lifetime of channeled dimmings can reach several hours.

We can note the following in connection with the identification of these large-scale channeled dimmings with observed coronal and photospheric features, based on a comparison of the difference images in Fig. 2a−2d with the H_α heliogram (Fig. 2e) and the original background (negative) image at 195 Å (Fig. 2f). The two main transequatorial dimming channels, 1−2 and 12−13−14, seem to coincide with the looplike transequatorial features observed at
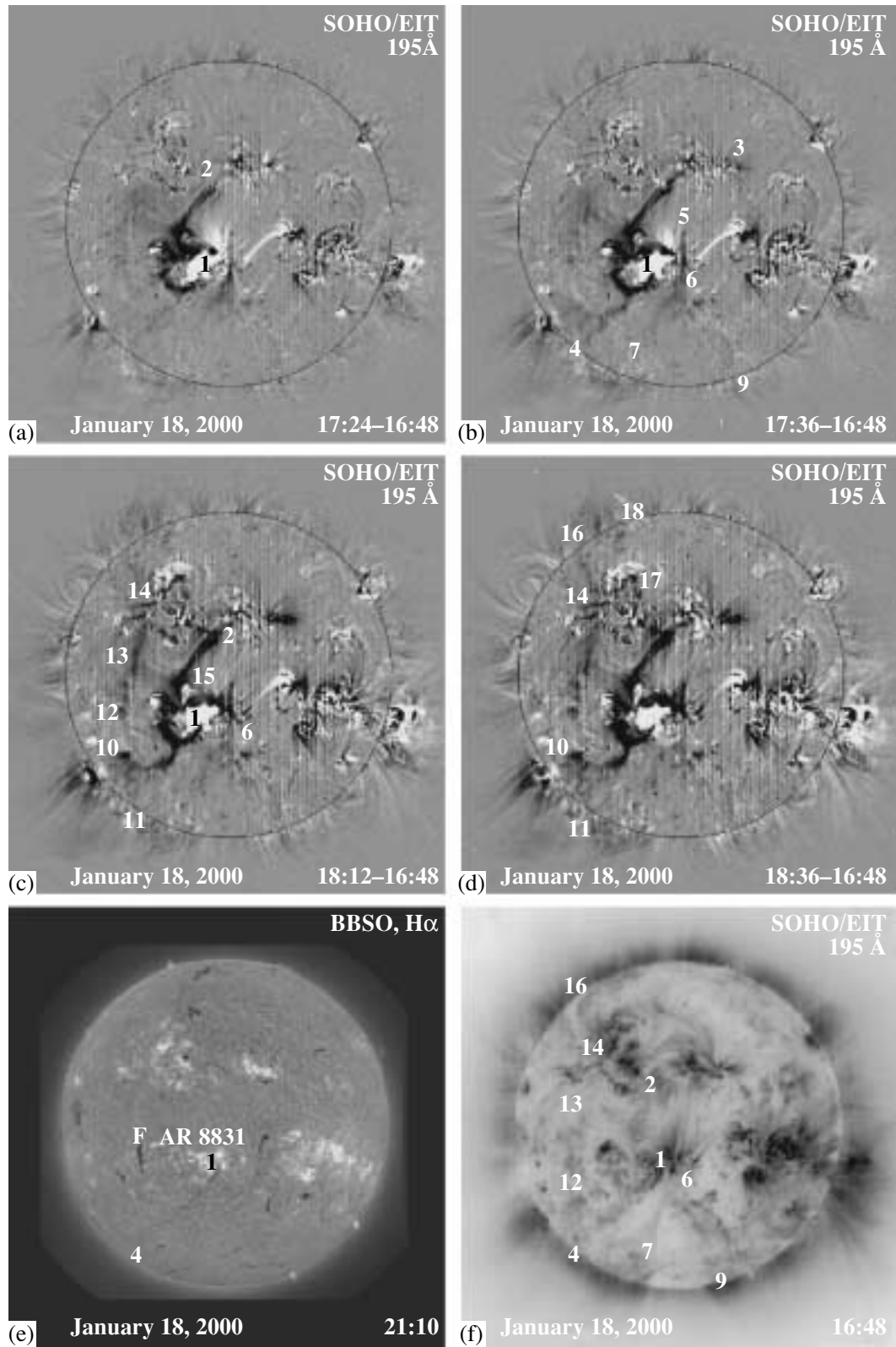
Fig. 2. (a–d) Fixed difference solar images in the 195 Å line for January 18, 2000 (SOHO EIT) obtained by subtracting the heliogram of 16:48 UT. These illustrate the halo-CME-related development of channeled dimmings with the presence of several activity centers on the disk. Bottom panels: (e) H$_\alpha$ heliogram; (f) original base (negative) image at 195 Å.
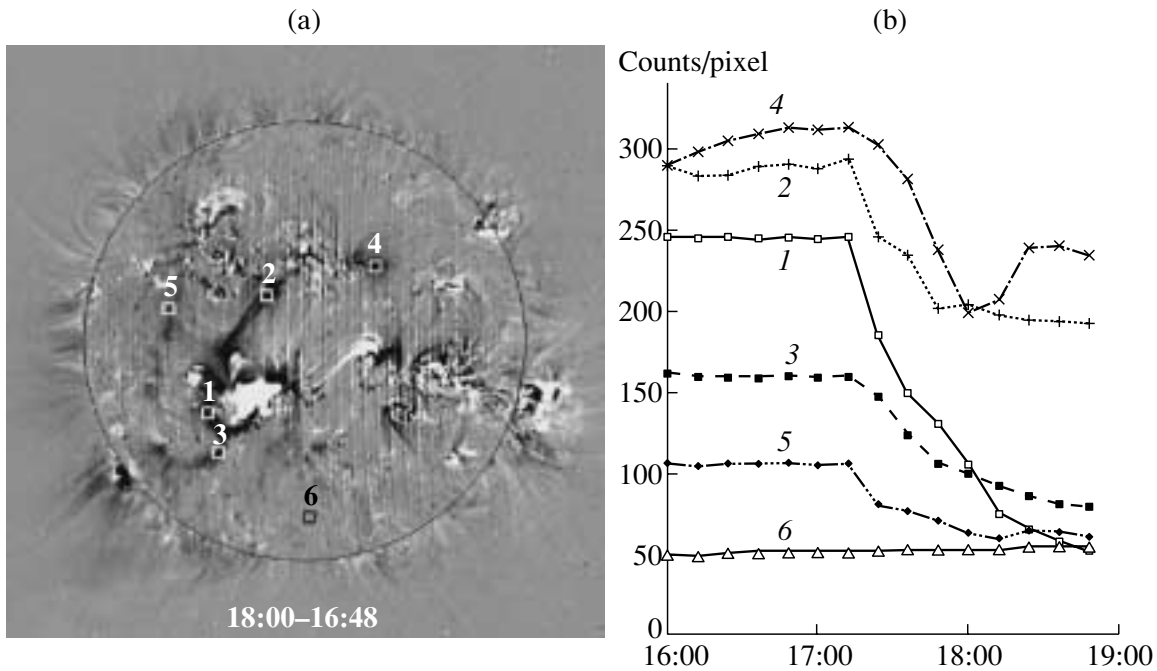
Fig. 3. (b) Time variation of the intensity in the 195 Å line during the event of January 18, 2000, for several 53″ × 53″ areas shown in panel (a): (*1−5*) in channeled dimmings and (*6*) in the southern coronal hole. The instrumental background has been subtracted.

195 Å and labeled by the same numbers in Fig. 2f. In addition, dimming 1−4 corresponds to the channel of the southeastern H$_\alpha$ filament (Fig. 2e), while dimmings 6−7, 6−9, and 14−16 are located along the western and eastern boundaries of the southern polar CH and the western boundary of the northeastern CH, respectively. Note that the H$_\alpha$ filament F (Fig. 2e), which is closest to the eruption center and is surrounded by dimming channels, did not exhibit obvious signatures of a disturbance related to this eruptive event.

It is characteristic of this event that no extended and bright coronal-wave front (in the usual sense) can be seen in either the FD or the RD movies, much less in the corresponding images. Instead, something like a dimming wave is observed: individual dimming channels and the entire region covered by dimmings become more extended with time. As this takes place, a few irregular, transient brightenings with small areas and intensities adjoin the dimming features. Estimates that can be obtained with a large interval between frame rate indicate that the propagation speed of this dimming wave is several hundred km/s, typical of classic bright coronal waves (see Section 3.1). It is important that the dimming wave in this event spread from the eruption center mainly eastward, northward, and southward, but essentially did not intersect the central meridian; i.e., it was not spherically symmetric.

3.3. Event of February 17, 2000

Among other things, this event is interesting because it occurred one solar rotation after the preceding one and at nearly the same site on the solar surface (Section 3.2), with the same complexity of the global solar magnetosphere. It developed against the background of two sympathetic flares of classes M2.5/1B and M1.3/2N, which occurred in the nearby active regions in the southern hemisphere AR 8869 and AR 8872 (S25 W16 and S29 E07; Fig. 4e) and reached their maxima in soft X rays at 18:52 and 20:35 UT, respectively. A number of arguments based on the optical, magnetic, UV, and X-ray data [34] suggest that the first flare initiated the second and that the two active regions were interconnected by magnetic structures. The annular transequatorial system of emitting chains 1−5−3−7−8−9−10−6, which can be seen in the processed SOHO EIT heliogram at 195 Å (Fig. 4f; a negative), indicates that this connection had a global character and encompassed all active regions located in the central sector of the disk [31]. According to the SOHO LASCO coronagraph data, the first manifestations of a CME were observed over the southwestern limb at 19:31 UT, and a symmetric halo CME developed around the entire occulting disk after 20:06 UT. This symmetric CME configuration seems to reflect the fact that, as will be shown below, the eruption process involved a similarly shaped, circular central region of

the disk depicted by the chain 1–5–3–7–8–9–10–6, together with the system of channeled dimmings that can be seen in the FD images (Figs. 4a–4d) and corresponding movies.

During the first flare, the connection between regions AR 8869 and AR 8872 was marked by two dimming structures (Fig. 4a). One was relatively wide and connected the western extremity of dimming 1, flare brightening 2, and the eastern region 3, and extended to the southeast in the form of the narrow channel 3–4. The other was a narrow arc, 1–5–3, and curved around the flare region from the south. Furthermore, at this stage, a faint dimming encompassed the entire central region of the disk between regions 2, 3, 7, 8, 9, 10, and 6. The somewhat deeper but nevertheless faint transequatorial dimming channels 1–9, 3–9, and 6–10 stood out against this background. Channels 1–9, 6–10, and dimmings 7–8, 8–9 were seen at a late stage of the first flare (Fig. 4b). By that time, flare brightening 2 increased its longitudinal extent, and the first signs of the second flare appeared in region 3; the wide dimming 2–3 between the interacting active regions almost vanished, while channel 2–11 connecting the brightening 2 with the southern arclike dimming 1–5–3 became more pronounced.

The second flare was accompanied by the emergence of new dimmings around the bright feature 3 (Fig. 4c). The looplike dimming systems 12 and 13 formed to the northeast and south of this feature. The western base of these dimming systems abutted on region 11, through which passed the narrow channel related to the first flare 2 and the enhanced eastern branch 3–5 of the arclike dimming 1–5–3. The well-defined dimming channel 3–14 with several branches formed north of the flare region, in the direction of region 9. Substantial enhancements were observed in many channeled dimmings localized in the central zone of the disk, including areas between the regions 3–8, 8–9, 1–9, and 1–10. All these dimming features developed further in the final stage of the event (Fig. 4d). In particular, the continuation of the brightest transequatorial channel 3–14 toward region 9 became quite prominent. The depth of the dimmings situated to the south of this region and those stretching to the eastern region 8 increased substantially. The emergence of dimmings going from the second flare brightening 3 to the southeastern limb 15 (with branching from point 16 to region 7) and to the southern limb 17 (with a deep dimming center observable outside the solar disk) was noted. Toward this same region, dimming 5–17 stretched from the area of the first flare through the western part of the arclike channel 1–5. Channeled dimmings formed east of regions 7 and 8, reaching points 18, 19, and 20. Narrow dimmings can also be seen between

regions 1, 10 and 7, 8. Dimming fragments are visible between region 9 and the northern limb 21.

Curves describing the development and depth of the dimmings within several key $53'' \times 53''$ areas are shown in Fig. 5. We can clearly see a time lag between the emergence of the dimmings related to the first and second flares. The first flare was accompanied by the onset of dimmings at about 19 UT in areas 1, 2, and, partially, 3. Significant dimmings are related to the second event, beginning at 20:20–20:40 UT in areas 5 and 6 related to the meridional channel, in the southern area 4, and again in area 3. The onset of the dimming in the northern area 6 was appreciably delayed. Curve 7, which is shown for comparison and verification purposes, demonstrates a smooth intensity decrease in the area over the southwestern limb, which does not seem to be related to the dimmings considered here. As in the preceding event, the depths of the main and channeled dimmings are tens of per cent, while the development time comprises several tens of minutes.

A comparison of the dimmings described above (Figs. 4a–4d) and the background heliogram at 195 Å (Fig. 4f; a negative) shows that the locations and configurations of most of the channeled dimmings correspond to elements of the annular system of emitting chains 1–5–3–8–9–10–6, which was observed prior to the event in the central portion of the disk. The deepest dimmings appeared precisely in the regions where the preflare UV features had been brightest. For example, the southern arclike dimming channel 1–5–3 coincided with the corresponding bright chain between two flare regions. The deepest portions of the transequatorial dimming 3–9 and adjacent branches can be identified with features of increased intensity in the neighborhood of the southern and northern active regions. The diagonal dimming 1–9, as well as the eastern and western meridional dimmings 7–8 and 1–10, were located at the sites of corresponding UV features. The dimming fragments localized outside the central zone and extending southward from the flare regions 2 and 3, eastward from regions 7 and 8, and northward from region 9 also had counterparts in the background heliogram, in the form of features of increased intensity.

It is clear from these data that, as in the preceding case, the disturbances related to the halo CME under consideration were global and anisotropic. This is true not only of the dimmings, but also of the coronal wave. As indicated by the movies of the FD and RD images, some manifestations of the coronal wave and traveling dimmings can be detected only within the southern sector bounded by elements 3–16–15 and 5–17 (Fig. 4d). In addition, modest-sized, fragmentary brightenings accompanied the development of
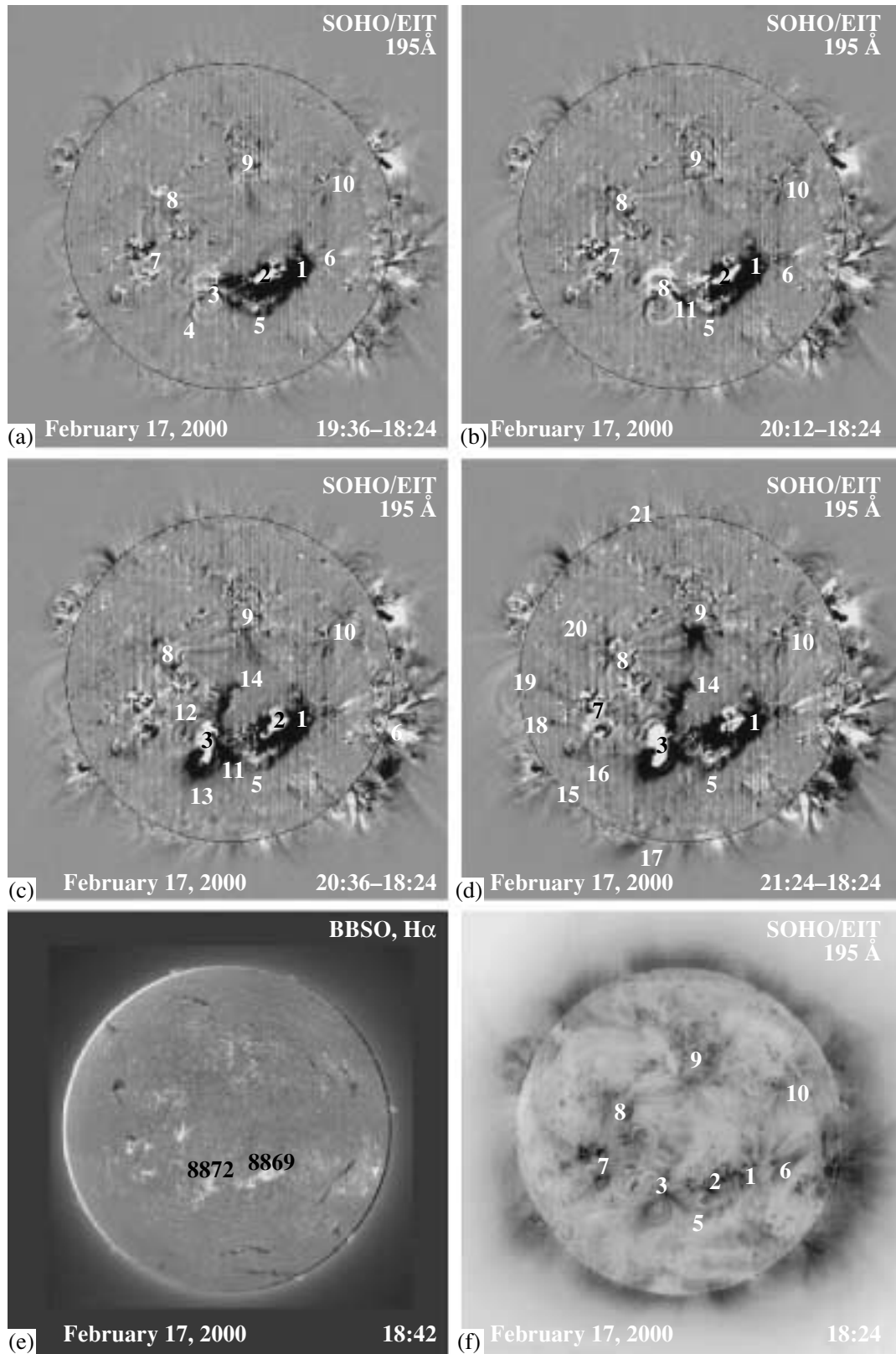
Fig. 4. (a–d) Fixed difference solar images in the 195 Å line for February 17, 2000 (SOHO EIT) obtained by subtracting the heliogram of 18:24 UT. These illustrate the development of channeled dimmings after the halo CME and two sympathetic flares. Bottom panels: (e) H$_\alpha$ heliogram; (f) original base (negative) image at 195 Å.

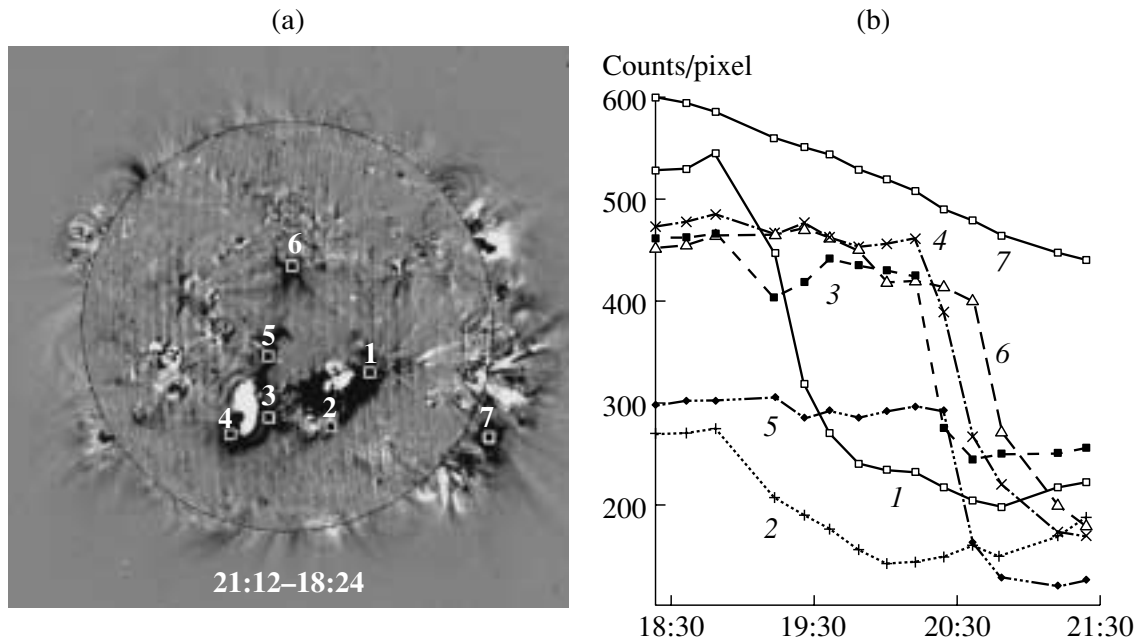(a)   (b)

Fig. 5. (b) Time variation of the emission intensity in the 195 Å line during the event of February 17, 2000, for several $53'' \times 53''$ areas shown in panel (a): (*1, 3, 4*) in dimmings adjacent to the flare centers and (*2, 5, 6*) in channeled dimmings. For comparison and verification purposes, the intensity variation in region (*7*) over the southwestern limb is also shown. The instrumental background has been subtracted.

the transequatorial dimmings 1−9 and 3−9 in the central zone of the disk.

4. DISCUSSION AND CONCLUSION

Our analysis of the difference UV SOHO EIT heliograms (primarily the FD images) at 195 Å suggests the following properties of halo-CME-related, large-scale solar dimmings and coronal waves.

There are events in which isotropic dimmings and coronal waves are observed developing more or less symmetrically in all directions from the eruption center [15, 17].

Here, we have identified events with pronounced anisotropic dimmings localized along a number of narrow, extended structures—channels.

Such channeled dimmings extend between widely separated activity centers, including those located on either side of the heliographic equator, and cover the visible solar disk almost entirely; in other words, they are global disturbances.

The reduction in the intensity of EUV emission in many dimming channels is comparable to that in isotropic dimmings and reaches several tens of per cent.

Channeled dimmings develop within several tens of minutes and can exist for several hours, as do dimming elements around eruption centers.

In channeled-dimming events, bright coronal waves are either not observed at all or are also anisotropic and propagate within a restricted sector of the disk. In some cases, a wave of dark dimmings is observed instead of a bright coronal wave.

Estimates based on the available data indicate that the propagation speeds of both channeled dimmings and coronal waves are several hundred km/s.

The appearance of isotropic or channeled dimmings apparently depends on the level of complexity of the global solar magnetosphere.

Isotropic dimmings and coronal waves are observed when the structure of large-scale magnetic fields is simple, when only one activity center present on the solar disk.

In contrast, channeled dimmings and anisotropic coronal waves are typical of complex structures of the global solar magnetosphere, with the presence of several active regions, filaments, coronal holes, etc. on the disk.

Only preliminary remarks about the identification of dimming channels with coronal structures can be made at this time. It is obvious that channeled dimmings outline or curve around existing large-scale coronal structures. Some dimming channels appear to coincide with pre-CME looplike transequatorial emission features observed in the same line, 195 Å, between widely separated active regions. A similar halo-CME-related reduction in the intensity

of transequatorial X-ray and UV loops was noted in [27] (see also [22, 28, 29]). In some cases, channeled dimmings arise at the scene of large-scale emitting UV chains [31]. Such channeled dimmings can probably be regarded as transient chains in absorption. Extended dimmings may also be aligned with the H_α filament channel. Just as coronal waves avoid active regions [26] and stop in front of CHs [15], channeled dimmings do not penetrate into CHs, and remain localized along their boundaries.

The detected channeled dimmings provide additional evidence that widely separated active regions and other features, including those situated in different solar hemispheres, are integrated into a single, complex system that forms the global solar magnetosphere. Large-scale emission chains also provide evidence for this idea, and some seem to trace out quasi-separatrix layers between different interacting magnetic fluxes in the global solar magnetosphere (see [31]).

The observations clearly indicate that, during a major CME, a substantial portion of the global solar magnetosphere becomes involved in the eruption process within several tens of minutes. This probably refers first and foremost to structures that are directly magnetically linked to the eruption center [29]. It is also not ruled out that these phenomena are induced by an MHD disturbance that spreads from the eruption center and is identified as a coronal wave.

It is obvious that the deepest dimmings affect structures that had fairly high emission measures and were sources of enhanced emission before the eruption. Dimmings and dimming channels demonstrate the presence of well defined coronal features and extended structures in the complex global solar magnetosphere, which exhibit the most pronounced CME-related intensity decreases. Such decreases could result from a partial or complete opening of the magnetic field lines in the process of the CME, with an associated evacuation of material. Another possibility is that an originally isotropic MHD disturbance affects these structures. It is likely that one or the other (or both) of these factors—the opening of field lines or an MHD disturbance—operate in specific events or in specific regions of the global solar magnetosphere.

On the whole, we can conclude that channeled dimmings are an important consequence and indicator of strong disturbances and substantial restructurings of large-scale features of the global solar magnetosphere in the corona during and after a CME. Further analyses are needed to gain a more comprehensive understanding of the nature of channeled dimmings and their role in CME processes.

REFERENCES

1. I. M. Chertok, Astron. Zh. **70**, 165 (1993) [Astron. Rep. **37**, 87 (1993)].
2. A. J. Hundhausen, in *The Many Faces of the Sun,* Ed. by K. Strong *et al.* (Springer-Verlag, New York, 1999), p. 143.
3. D. F. Webb, J. Atmos. Sol.-Terr. Phys. **62**, 1415 (2000).
4. M. D. Andrews and R. A. Howard, Space Sci. Rev. **95**, 147 (2001).
5. H. S. Hudson and E. W. Cliver, J. Geophys. Res. **106**, 25199 (2001).
6. J. A. Klimchuk, in *Space Weather,* Ed. by P. Song, H. Singer, and G. Siscoe (AGU, Washington, 2001), Geophysical Monograph, No. 125, p. 143.
7. Y. Ogawara, T. Takano, T. Kato, *et al.*, Sol. Phys. **136**, 1 (1991).
8. V. Domongo, B. Fleck, A. I. Poland, *et al.*, Sol. Phys. **162**, 1 (1995).
9. G. E. Brueckner, R. A. Howard, M. J. Koomen, *et al.*, Sol. Phys. **162**, 357 (1995).
10. S. Tsuneta, L. Acton, M. Bruner, *et al.*, Sol. Phys. **136**, 37 (1991).
11. J.-P. Delaboudinière, G. E. Artzner, J. Brunaud, *et al.*, Sol. Phys. **162**, 291 (1995).
12. D. M. Rust, Space Sci. Rev. **34**, 21 (1983).
13. A. C. Sterling and H. S. Hudson, Astrophys. J. **491**, L55 (1997).
14. H. S. Hudson and D. F. Webb, in *Coronal Mass Ejections,* Ed. by N. Crooker, J. Joselyn, and J. Feynman, AGU Geophysical Monograph Series, No. 99, 27 (1997).
15. B. J. Thompson, S. P. Plunkett, J. B. Gurman, *et al.*, Geophys. Res. Lett. **25**, 2465 (1998).
16. D. M. Zarro, A. C. Sterling, B. J. Thompson, *et al.*, Astrophys. J. **520**, L139 (1999).
17. N. Gopalswamy and B. J. Thompson, J. Atmos. Sol.-Terr. Phys. **62**, 1427 (2000).
18. B. J. Thompson, J. B. Gurman, W. M. Neupert, *et al.*, Astrophys. J. **517**, L151 (1999).
19. A. Klassen, H. Aurass, G. Mann, *et al.*, Astron. Astrophys. **141**, 357 (2000).
20. D. A. Biesecker, D. C. Myers, B. J. Thompson, *et al.*, Astrophys. J. **569**, 1009 (2002).
21. B. J. Thompson, B. Reynolds, H. Aurass, *et al.*, Sol. Phys. **193**, 161 (2000).
22. A. Warmuth, B. Vršnak, H. Aurass, *et al.*, Astrophys. J. **560**, L105 (2001).

23. G. E. Moreton and H. E. Ramsey, Publ. Astron. Soc. Pac. **72**, 357 (1960).

24. C. Delannée and G. Aulanier, Sol. Phys. **190**, 107 (1999).

25. C. Delannée, Astrophys. J. **545**, 512 (2000).

26. L. Ofman and B. J. Thompson, Astrophys. J. **574**, 440 (2002).

27. J. I. Khan and H. S. Hudson, Geophys. Res. Lett. **27**, 1083 (2000).

28. S. Pohjolainen, D. Maia, M. Pick, *et al.*, Astrophys. J. **556**, 421 (2001).

29. T. Wang, Y. Yan, J. Wang, *et al.*, Astrophys. J. **572**, 580 (2002).

30. G. E. Brueckner, J.-P. Delaboudinière, R. A. Howard, *et al.*, Geophys. Res. Lett. **25**, 3019 (1998).

31. I. M. Chertok, Sol. Phys. **198**, 367 (2001).

32. S. P. Plunkett, B. J. Thompson, R. A. Howard, *et al.*, Geophys. Res. Lett. **25**, 2477 (1998).

33. D. F. Webb, R. P. Lepping, L. Burlaga, *et al.*, J. Geophys. Res. **105**, 27251 (2000).

34. H. Wang, V. Yurchyshyn, J. Chae, *et al.*, Astrophys. J. **559**, 1171 (2001).

Translated by A. Getling